coatings

MDPI

Article

A Comparison Study on the Microstructure, Mechanical Features, and Tribological Characteristics of TiN Coatings on Ti6Al4V Using Different Deposition Techniques

Zhen Liu [1], Shuai Ren [1], Tijun Li [2,*], Pinghu Chen [3,*], Liangbin Hu [3], Wenxing Wu [3], Sheng Li [3], Hao Liu [4], Ruiqing Li [5] and Yun Zhang [6]

1 College of Mechatronics and Control Engineering, Shenzhen University, Shenzhen 518060, China; liuzhen598352368@126.com (Z.L.); shuai.ren@szu.edu.cn (S.R.)
2 State-Owned Sida Machinery Manufacturing Company, Xianyang 610400, China
3 Key Laboratory of Hunan Province of Equipment Safety Service Technology under Extreme Environment, College of Mechanical Engineering, College of Nuclear Science and Technology, School of Resource Environment and Safety Engineering, University of South China, Hengyang 421001, China; huliangbin83@sina.com (L.H.); wuzhiaifrank@hotmail.com (W.W.); lisheng325@126.com (S.L.)
4 College of Mechanical Engineering, Hunan Institute of Engineering, Xiangtan 411104, China; liuhao10212510@163.com
5 State Key Laboratory of Precision Manufacturing for Extreme Service Performance, Light Alloys Research Institute, Central South University, Changsha 410083, China; liruiqing@csu.edu.cn
6 School of Mechanical Engineering, Hunan University of Science and Technology, Xiangtan 411201, China; yun_zhang66@163.com
* Correspondence: litj@pku.edu.cn (T.L.); chenpinghu1986@163.com (P.C.)

Abstract: Titanium alloys are considered lightweight alloys and are widely applied across various industries. However, their low hardness, poor wear resistance, and limited oxidation resistance restrict their prospects for wider application. In this paper, nitride coatings were prepared using three preparation processes, namely laser surface nitriding (LSN), physical vapor deposition (PVD), and plasma ion implantation (PII). Their microstructure, microhardness, tribological behavior, and high-temperature oxidation characteristics were compared. The experimental results revealed that nitrided coatings were successfully prepared using the three methods. However, a comparison of these data shows that the LSN coating exhibited superior comprehensive performance. It achieved the maximum thickness within the shortest preparation time: the thickness was about 280 μm and the deposition rate of the LSN method was 2250 and 90,000 times higher than those of the PVD and PII methods. Nitrides have high hardness, but the carrying capacity could be attributed to the thickness of the coatings: the PVD coating could withstand a force of 500 g, while the PII coating only withstood a force of less than 25 g. In addition, as hardness is the most important factor for excellent wear resistance, the average volumetric wear rate of the LSN and PVD coatings was about 9×10^{-6} $mm^3/m{\cdot}N$, and their relative wear resistance was 49.2 times that of Ti6Al4V. Meanwhile, the excellent bond between the LSN coating and the substrate was evidenced by a high-temperature oxidation test during a rapid heating–cooling cycle.

Keywords: Ti alloys; surface nitriding; microhardness; wear resistance; high-temperature oxidation resistance

Citation: Liu, Z.; Ren, S.; Li, T.; Chen, P.; Hu, L.; Wu, W.; Li, S.; Liu, H.; Li, R.; Zhang, Y. A Comparison Study on the Microstructure, Mechanical Features, and Tribological Characteristics of TiN Coatings on Ti6Al4V Using Different Deposition Techniques. *Coatings* **2024**, *14*, 156. https://doi.org/10.3390/coatings14020156

Academic Editor: Alessandro Patelli

Received: 7 December 2023
Revised: 19 January 2024
Accepted: 22 January 2024
Published: 24 January 2024

1. Introduction

Titanium and its alloys have the advantages of low density, high strength, good corrosion resistance, etc., and they are used in the automobile, aerospace, military, and biomedical industries [1–4]. However, low hardness and susceptibility to wear limit their wide application [5–7]. Especially in aerospace, a complex service environment (ocean or desert zone) can cause a deterioration of mechanical properties and early failure [8–10].

Therefore, the requirement for lightweight in key transmission pairs restricts the use of titanium alloys in aircraft [11]. To meet the needs of industrial applications, titanium alloys should be enhanced for excellent wear resistance through different methods, such as novel materials development, surface alloying, and coating techniques.

A novel Ti alloy with high hardness was designed by Chen, P.H. [12]. The refractory high entropy alloy $Ti_{30}Hf_{20}Nb_{20}Ta_{10}V_{10}Mo_7W_3$, with excellent wear resistance, was designed by Wei, Q. [13]. The Cu element was added to the Ti-10Mo alloy to improve microhardness and tribo-corrosion resistance [14]. Two medium-entropy alloy coatings were prepared on a CP-Ti sheet by pulsed laser cladding, achieving a hardness of 762 HV and a specific wear rate of 1.7×10^{-5} $mm^3 \cdot N^{-1} \cdot m^{-1}$ [15]. A NiTi coating was prepared by the tungsten inert gas (TIG) cladding process, resulting in a microhardness of 680 $HV_{0.05}$ to enhance the wear resistance of the Ti6Al4V substrate [16]. Pure boron powders were pre-placed on the surface of the Ti6Al4V substrate, and high-hardness TiB, AlTi, $AlTi_2$, and $AlTi_3$ were precipitated to improve wear resistance [17]. An oxygen-charging method was employed to fabricate β-Ti alloys with ultrahigh surface hardness and exceptional wear resistance [18]. In addition, laser shock peening was performed to enhance the impact wear behavior of the Ti6Al4V substrate [19]. The ball burnishing process was applied to minimize the friction coefficient and increase micro-hardness, achieving a specific wear rate decrease of 52% as compared to Ti6Al4V [20]. The duplex treatment of plasma Ti alloying and plasma nitriding was applied to prepare a TiN coating, thus resulting in better wear resistance on the surface of the C17200 alloy [21]. Rossi et al. reported that a hard surface was created on different titanium alloys by plasma nitriding treatment and compared their microhardness and wear resistance [22]. Compared with the aforementioned surface modification methods, surface nitriding treatment is one of the simplest methods to enhance wear resistance. However, it could introduce new issues, such as high costs or long manufacturing cycles.

In this paper, to obtain a coating with high hardness for wear resistance, three nitriding methods were employed, namely laser surface nitriding (LSN), physical vapor deposition (PVD), and plasma ion implantation (PII), to deposit coatings on the Ti6Al4V substrate. Scanning electron microscopy (SEM), X-ray diffraction (XRD), and energy dispersive spectroscopy (EDS) were applied to analyze the microstructure and phases. The relationship between the thickness and deposition time was discussed to assess the thickness and deposition efficiency of the coatings. Microhardness and tribological behaviors were measured using a Vickers hardness tester and a high-temperature friction-wear machine. Meanwhile, the bonding strength was explored by high-temperature oxidation testing. And the microstructure, mechanical properties, and tribological behaviors of the coatings deposited by different methods were compared in detail.

2. Materials and Methods

A Ti6Al4V alloy was used as the substrate in this work, cut into rectangular blocks measuring 20 mm × 20 mm × 5 mm. The surfaces of all samples were polished using metallographic sandpaper with 400, 800, 1200, 1500, 2000, and 5000 mesh and polishing suspension with 0.5 μm diamonds, followed by drying for use. Firstly, the HEMII-80 ion implanter (Plasma Technology Ltd., Hong Kong, China) was utilized to conduct N ion implantation, as depicted in the schematic diagram reported in Refs. [23,24]. Before implantation, the plates were sputter-cleaned using argon plasma ion bombardment. During implantation, N_2 was introduced into the vacuum chamber, maintaining N plasma at a power of 900 W, a working pressure of 8×10^{-2} Pa, and a gas flow of 25 mL/min. Ion implantation was conducted at an accelerating voltage of 2 kV for 2.5 h at a base pressure of 1×10^{-3} Pa, with an N ion implantation dose of ~4×10^{17} ions/cm^2. Secondly, a TN target was supplied by Beijing Hezong Technology Co., Ltd., and a TSU-650 multifunctional coating machine (PVD technique, as in a previously reported schematic diagram [25]) was used to prepare the TiN coating. This process included a substrate bias voltage of ~100 V, target current of 1.3 A, a deposition time of 300 min, a duty cycle of 50%, a target base

distance of 170 mm, and a substrate temperature of 300 °C. Thirdly, the XL-500 Laser cladding system (Guangzhou Xinglai Laser Technology Co., Ltd., Guangzhou, China) was adopted, equipped with a 500 W laser with a pulse width of 10–50 ns. The laser parameters included a power of 36 W, a scanning speed of 1800 mm/min, and a lapping rate of 90%; the deposition time was about 3 min (a similar schematic diagram was reported in Ref. [26]). In addition, the reaction atmosphere of high-purity N_2 at 99.99% with a 10 L/min flow rate was maintained during laser surface nitriding. The treated samples are referred to as PII, PVD, and LSN coatings, with detailed deposition method information presented in Table 1.

Table 1. The working parameters of three deposition methods.

Method	Process Parameters						
LSN	Power 36 W	Scanning speed 1800 mm/min		Lapping rate 90%		Deposition time 3 min	N_2 Flow rate 10 L/min
PVD	Target TiN	Target distance 170 mm	Substrate preheat 300 °C	Target current 1.3 A	Bias voltage ~100 V	Deposition time 300 min	Duty cycle 50%
PII	Power 900 W	Work pressure 8×10^{-2} Pa	Voltage 2 kV	Base pressure 1×10^{-3} Pa	Ion dose ~4×10^{17} ions/cm^2	Deposition time 150 min	Gas flow 25 mL/min

Microhardness on the surface of different coatings was measured using a Vickers hardness tester (Micro Vickers HV1000Z, MEGA INSTRUMENTS, Shanghai, China). Various forces of 10 g, 25 g, 100 g, 200 g, and 500 g were applied to obtain the microhardness value and carrying capacity. For each coating, 5 points were measured, and their average value was taken as the final result. The high-temperature friction-wear machine (HT-1000, Zhongke Kaihua, Lanzhou, China) was employed to measure wear characteristics [27], with testing parameters set as follows: a friction force of 3 N, a friction speed of 500 r/min, a rotation radius of 4 mm, a friction time of 30 min, and a φ6 mm Si_3N_4 counterpart ball. And then the mechanical profiler was utilized to delineate the wear tracks, and the average wear volume was calculated based on data collected four times at quarter positions. The volume wear rate was expressed by the equation $w = V/(F \cdot L)$ [28], where w is the volume wear rate ($mm^3/m \cdot N$), V is the wear volume (mm^3), F is the friction force (N), and L is the run length (m). To explore the bonding between the coatings and substrate, an individual oxidation test was performed in an electric resistance furnace, similar to the test reported in Ref. [29]. Firstly, the furnace temperature was heated and stabilized at 700 °C. Secondly, the samples were placed in the furnace for holding times of 5 and 10 h, and the surface characteristics after high-temperature oxidation were characterized using a digital camera.

A high-energy X-ray diffractometer (HE-XRD, D8 discover, Bruker, Karlsruhe, Germany), using Cu-Kα radiation (λ = 0.15418 nm), was employed to examine the phase constitutions of the coatings deposited by different methods. The device was operated at 40 kV and 80 mA over a 2θ range of 30–80°, with a scanning rate of 2°/min. The microstructure of the surface and cross-section was characterized by scanning electron microscopes (SEM, TESCAN MIRA three LMH/LMU, Brno, Czech Republic). In addition, energy-dispersive X-ray spectroscopy (EDS) was utilized to determine the elemental distribution in the cross-section.

3. Results and Discussion

Figure 1 shows the XRD patterns of the samples deposited by different methods. The phase components of the three coatings differ significantly owing to different preparation processes. High crystallinity occurs on the surface of the sample fabricated by laser surface nitriding. The black line in Figure 1 indicates that abundant titanium nitride (TiN), a few aluminum nitride (AlN), and hcp-Ti can exist on the coating. The PVD coating exhibits broad peaks indicating, on the one hand, that crystallinity is relatively low under the current parameter conditions. On the other hand, a single peak contains three peaks from different phases; for example, the (111) crystal plane (111) of Vanadium nitride (VN), (111) of TiN, and (100) of hcp-Ti appear at ~36°. However, abundant hcp-Ti is discovered on the surface of the PII sample, with only a small presence of TiN and AlN detected. When

comparing the three samples, the peak intensity of hcp-Ti gradually increased from the LSN coating to the PII coating. This can be because a difference exists in the thickness and surface characteristics of the coatings.

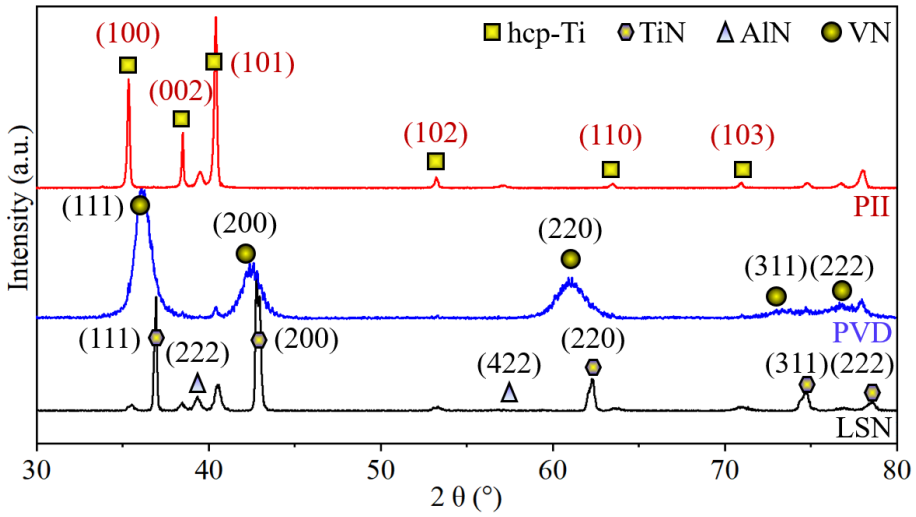

Figure 1. XRD patterns of the samples deposited by different methods.

Just as shown in Figure 2, the surface and cross-section microstructure of the samples with different methods used. High energy can contribute to the reaction region where nitrides are formed in situ owing to the embedment of supersaturated N_2. Obvious laser scanning traces are visible on the surface of the LSN sample, as shown in Figure 2a; the width between the two traces is about 100 μm, and holes and cracks appear. The surface roughness is also the maximum because of the violent fluctuation within the molten pool caused by high energy density. Meanwhile, the cross-section morphology shows obvious stratification in the coatings, consisting of a loose upper layer, a compact middle layer, and a transition layer, with a total thickness of about 280 μm. The deposition rate is determined by the relationship between the thickness and deposition time, with the values for LSN, PVD, and PII coatings being 70, 0.04, and 0.001 μm/min, respectively. This indicates that the deposition rate of the LSN coating is the highest, as shown in Table 2. Figure 2b reveals that some lateral and longitudinal cracks are present within the upper and middle layers. During X-ray diffraction testing, X-rays cannot penetrate the thick coating completely, resulting in a lower peak intensity of hcp-Ti in the sample fabricated by laser surface nitriding.

Table 2. The thickness of the coatings deposited by different methods.

Methods	Deposition Time (min)	Deposition Thickness (μm)	Deposition Rate (μm/min)
LSN	3	280	~70
PVD	300	11	~0.04
PII	150	0.19	~0.001

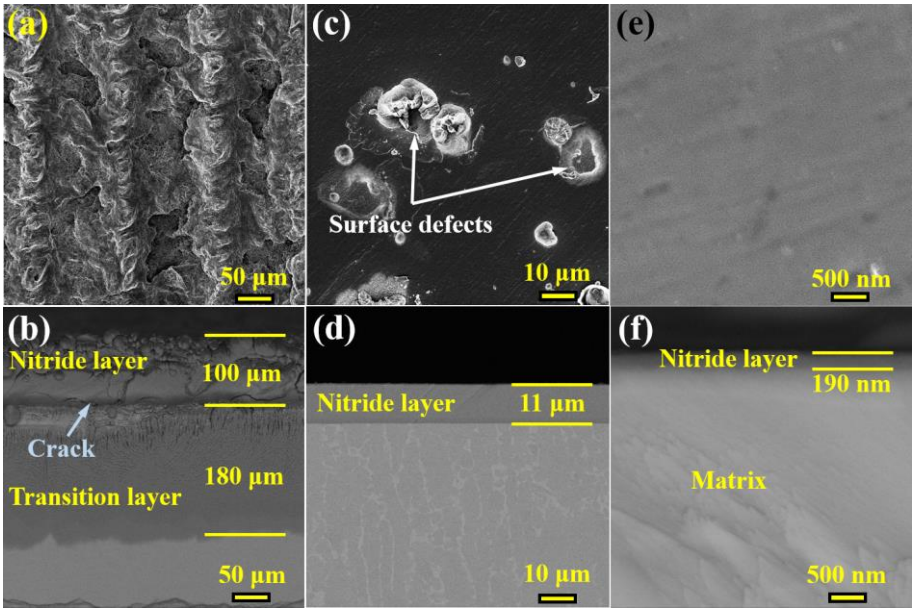

Figure 2. Surface and cross-section morphology of the samples deposited by different methods. (**a**,**b**) LSN; (**c**,**d**) PVD; (**e**,**f**) PII.

In the PVD sample, surface defects approximately ~20 μm in size are evident, as shown in Figure 2c. These defects can peel out during the preparation process. However, the cross-section morphology reveals that the ~11 μm coating is precipitated. It is incredibly dense, with a clearly defined interface between the coating and the Ti6Al4V substrate, as shown in Figure 2d. Just like the existence of the surface defects, a relatively high peak intensity of hcp-Ti is observed relative to the LSN sample. But fortunately, cracks were never discovered in the samples fabricated by PVD and plasma ion implantation. Due to the deposition rate of plasma ion implantation, only a 190 nm nitride layer is formed on the PII sample. Therefore, higher intensities of the hcp-Ti peaks are detected, indicated by a red line.

Figure 3 shows the elemental distributions in the line scanning of the cross-section for three samples. For the LSN sample, the upper layer includes AlN and TiN, but the TiN ratio can be higher in the transition layer, as shown in Figure 3a. More interestingly, an obvious AlN layer approximately 400 nm thick appears on the upper surface, and the AlN layer reappears at the interface between the coating and the Ti6Al4V substrate, as shown in Figure 3b. For the PII sample, VN can form in the 0.5–0.75 μm range from the top surface of the coating. These nitrides can contribute to microhardness and wear resistance. The microhardness of different samples under various forces is shown in Figure 4 and Table 3. The microhardness of Ti6Al4V is only 341.2 ± 8 $HV_{0.2}$; the microhardness values for PII, PVD, and LSN samples increase by 7%, 257.2%, and 274.1%, respectively. These values do not explain why the PII sample has low microhardness. We believe the coating of the PII sample is too thin to withstand the force. Therefore, a series of microhardness measurements were performed with different forces. The measured results reveal that a microhardness of 1260.8 ± 13 HV is obtained on the surface of the PII sample under the force of 10 g, with the average diagonal length on the top surface of the micro-indentation being about 3.88 μm according to the measured results (the facial angle of the indenter is 136°), yielding an indentation depth of about 554 nm. This depth is 2.9 times the thickness of the PII coating, yet the PII coating still has a preferable carrying capacity during the hardness test process. When the force is increased to 25 g, there is a 40.7% reduction in microhardness compared to the force of 10 g, with the depth of the indentation exceeding 1.1 μm, which indicates that the carrying capacity is weakened at 25 g. Table 3 reveals that the carrying capacity of the PVD sample can be up to 500 g, and that of the LSN

sample can be higher than 500 g, but testing above 500 g was not carried out owing to the rough surface.

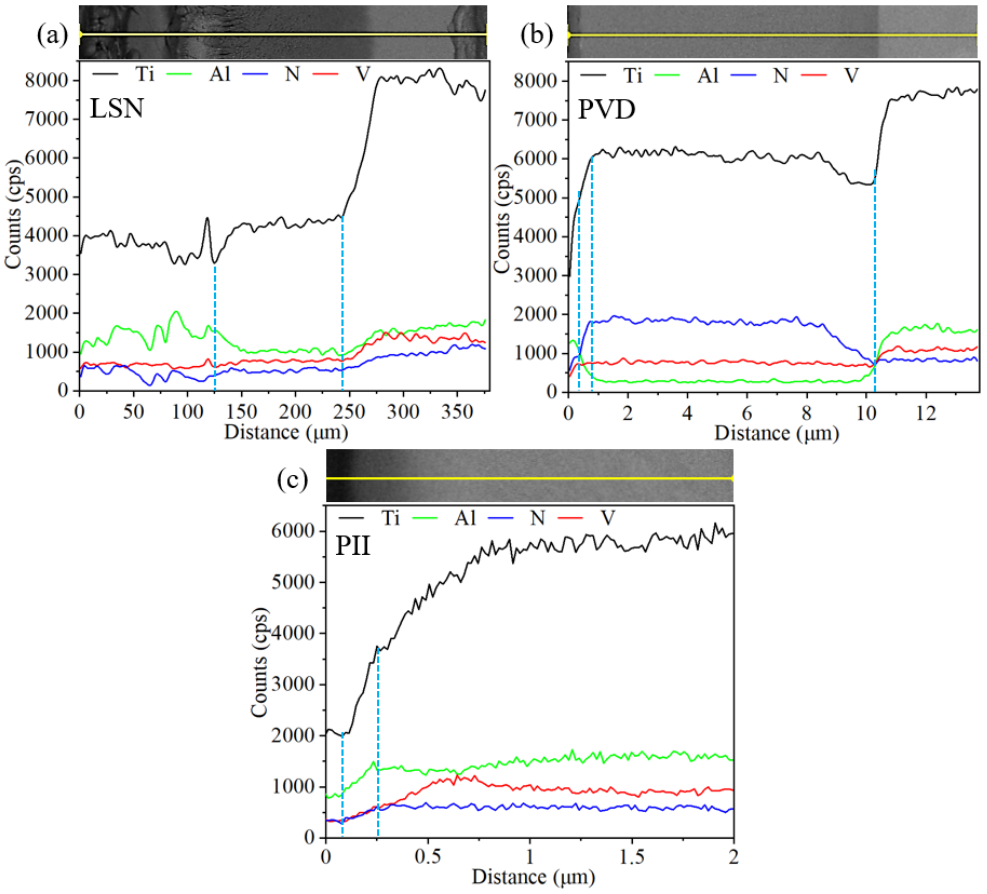

Figure 3. EDS elemental distribution in the cross-section of the samples deposited by different methods. (**a**) LSN; (**b**) PVD; (**c**) PII.

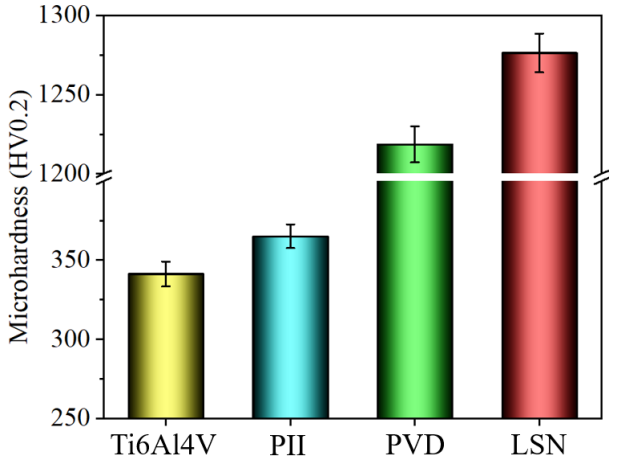

Figure 4. Microhardness of the samples deposited by different methods.

Table 3. Microhardness of the samples deposited by different loads.

Samples	Microhardness (HV)				
	10 g	**25 g**	**100 g**	**200 g**	**500 g**
Ti6Al4V	/	/	/	341.2 ± 8	/
PII	1260.8 ± 13	748 ± 10	377.5 ± 8	365 ± 8	351.7 ± 7
PVD	/	/	1597 ± 15	1218.6 ± 11	663 ± 10
LSN	/	/	1734.4 ± 21	1276.3 ± 12	/

It is well-known that hardness is one of the most important factors for wear resistance. Figure 5 shows the macro-scale morphology of the samples deposited by different methods. There is a huge difference in the characteristics of the wear tracks. A width of 1.16 mm is observed in the Ti6Al4V substrate, accompanied by a metallic color. A similar phenomenon occurs in the PII sample, with a width also about 1.16 mm and a metallic color, which indicates that the carrying capacity is low owing to the smaller thickness of the coating. The wear tracks of the PVD and LSN samples show a coated color. The width of the PVD and LSN samples decreased by 45.7% and 37.9%, respectively. This reveals that the coatings can withstand a wear force of 3 N given a certain thickness, and relatively excellent wear resistance is present in the PVD and LSN samples. Combined with the outline of the wear tracks in the different coatings, the most severe wear is seen on the Ti6Al4V substrate, where the depth of the wear track exceeds 30 μm. The nitride coatings can contribute to a relatively shallow wear track owing to their resistance to a 3 N wear force. However, in the PII coating, insufficient resistance can be caused by the ultrathin nitride coating, thus resulting in a depth of ~20 μm. Interestingly, the PVD and LSN coatings have excellent wear resistance with a wear track depth of ~1 μm, as shown in Figure 6. The volume wear rate was also obtained and is shown in Figure 7. A volume wear rate of 444 × 10^{-6} mm^3/m·N is observed in the Ti6Al4V, while the volume wear rates for the PII, PVD, and LSN coatings are 305 × 10^{-6} mm^3/m·N, 8.96 × 10^{-6} mm^3/m·N, and 9.02 × 10^{-6} mm^3/m·N, respectively. Their relative wear resistance is 1.45, 49.5, and 49.2 times higher than that of the Ti6Al4V substrate.

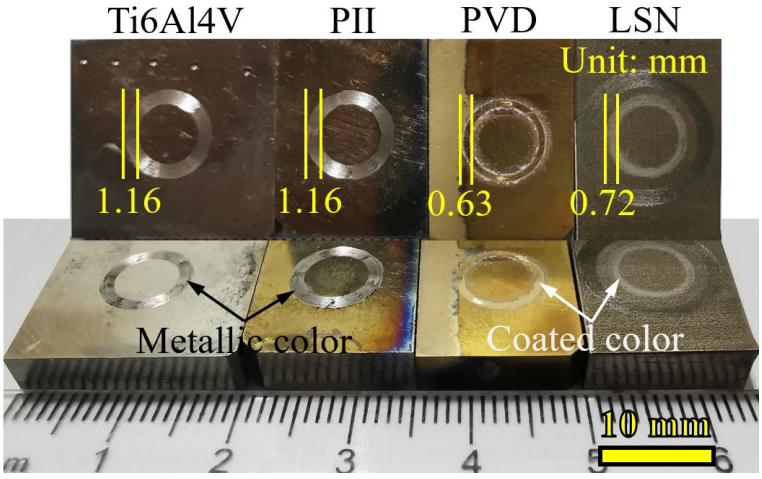

Figure 5. Macro-scale morphology of the samples deposited by different methods after friction-wear testing.

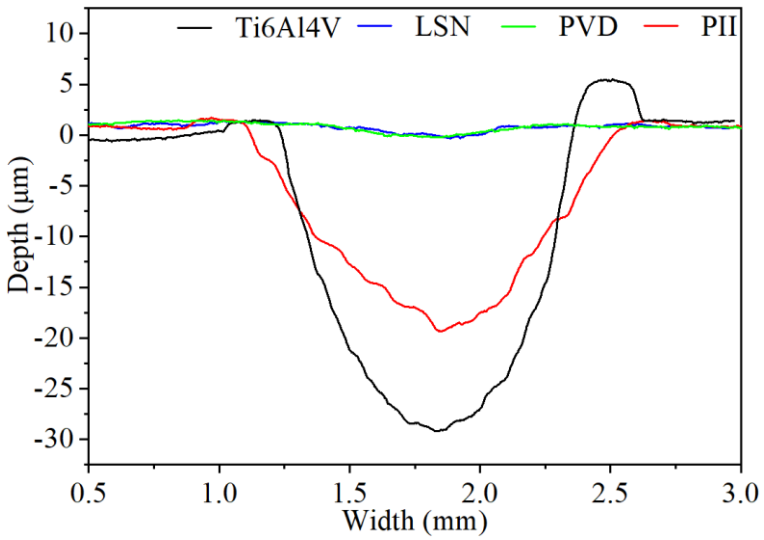

Figure 6. The outline of the wear tracks for the coatings deposited by different methods.

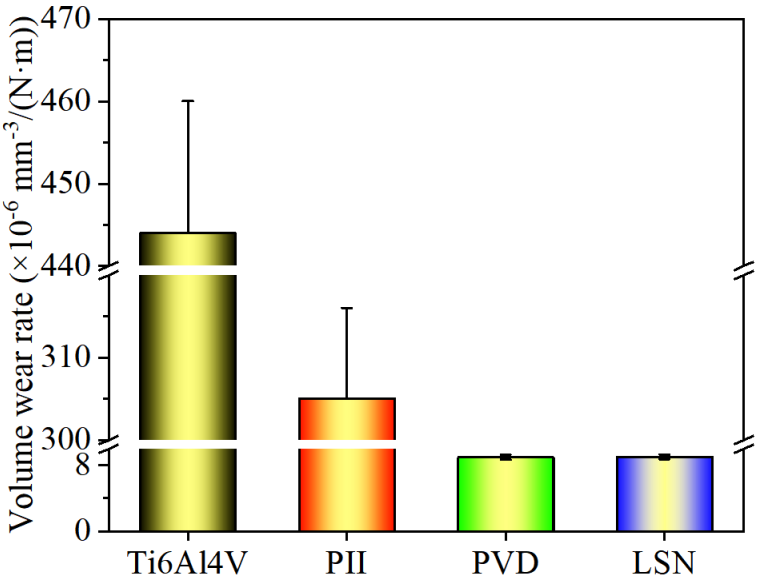

Figure 7. Average volume wear rate of the coatings deposited by different methods.

In addition to affecting hardness and wear resistance, the coating characteristics also contribute to high-temperature oxidation resistance. The affinity between titanium and oxygen is considerably high at high temperatures [30]. Ref. [31] reveals that a poor bond between the oxide layer and the base material causes serious spalling; this observation is consistent with our work, as shown in Figure 8a. For the LSN sample, obvious exfoliation is never observed in the LSN coating, but the oxidation phenomenon can occur in localized regions, as shown in Figure 8b. Vast areas of the nitride coating peel off after 5 h of oxidation, and a new oxide layer forms in the spalled areas, as shown in Figure 8(c2). This could be due to the preparation process; a clear interface between the PVD coating and Ti6Al4V substrate is noted, and poor bonding is an important factor causing spalling, owing to the hardness difference between the coating and substrate [32]. In addition, higher thermal stress can be another important factor for the failure of the coating during rapid heating–cooling cycles. The most important reason for spalling might be that some defects within the coating [25] act as channels for oxygen entering the substrate, primarily causing oxidation at the substrate, and the coating may crack and peel off owing to internal expansion caused by the formation of abundant oxides. A metallic bonding is evident

between the PII coating and the substrate. Therefore, high-temperature oxidation resistance is relatively higher; spalling begins at the surface edges after 5 h oxidation and continues to spread to the entire surface, as shown in Figure 8(d2).

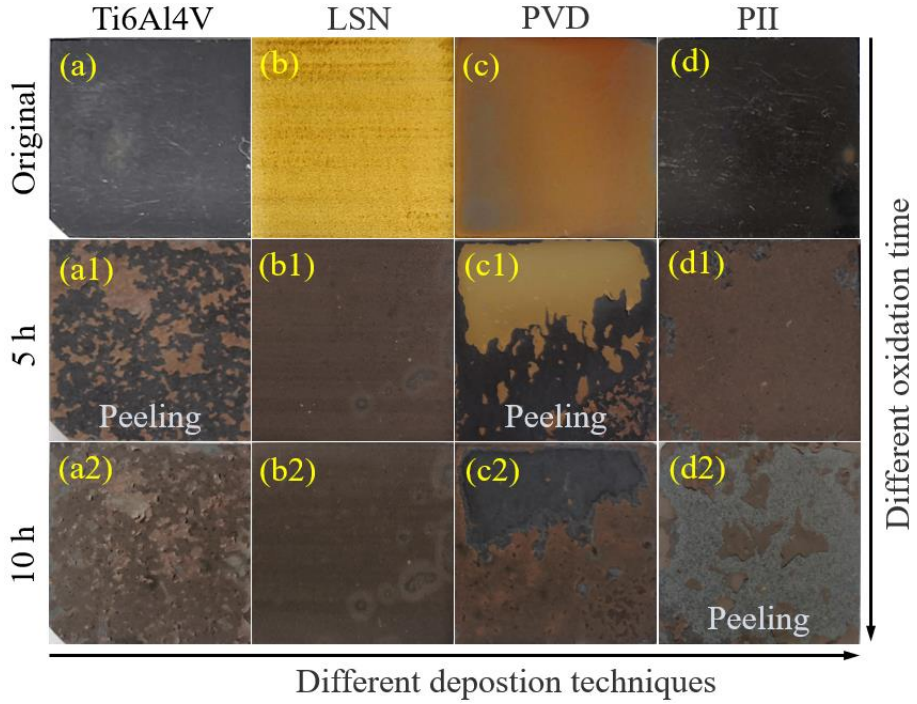

Figure 8. High-temperature oxidation of the samples deposited by different methods at 700 °C. (**a**) Ti6Al4V; (**b**) LSN; (**c**) PVD; (**d**) PII.

4. Conclusions

In this paper, three coatings were prepared using LSN, PVD, and PII on the Ti6Al4V. The microstructure, microhardness, wear behaviors, and high-temperature oxidation resistance were measured, and the main conclusions are as follows:

1. The nitriding coatings were successfully prepared. The LSN coating had the greatest roughness and thickness, with a thickness of about 280 μm, while the thicknesses of the PII and PVD coatings were 190 nm and 11 μm, respectively. The deposition rates for the LSN, PVD, and PII methods were about 90 μm/min, 0.04 μm/min, and 0.001 μm/min, respectively.
2. Owing to the thickness differences, the carrying capacities of the coatings varied significantly. The PII coating withstood forces of less than 100 g during microhardness testing. Relative to Ti6Al4V, the microhardness increased by 7%, 257.2%, and 274.1%, respectively.
3. Hardness and carrying capacity contribute to the wear resistance of the coatings. The volume wear rate of the Ti6Al4V substrate was only 4.44×10^{-4} $mm^3/m{\cdot}N$. The relative wear resistance of the PII, PVD, and LSN coatings was 1.45, 49.5, and 49.2 times higher than that of the Ti6Al4V substrate. The PVD and LSN coatings exhibited a wear rate of ~9.0×10^{-6} $mm^3/m{\cdot}N$.
4. Surface defects were present in the PVD coating; these could lead to the formation of oxides, which in turn could cause the coating to spall owing to differences in hardness, internal expansion, and thermal stress. Despite the presence of cracks in the LSN coating, it still had the best high-temperature oxidation resistance because a thick, dense layer impeded oxygen penetration. The excellent high-temperature oxidation resistance could be attributed to the metallurgical bonding.

Author Contributions: Conceptualization, Z.L. and T.L.; methodology, Z.L., L.H., S.L., H.L. and P.C.; software, Y.Z. and W.W.; validation, Z.L., R.L. and S.R.; formal analysis, W.W. and P.C.; investigation, Z.L., S.R. and T.L.; resources, T.L.; data curation, L.H., S.L., H.L. and P.C.; writing—original draft preparation, Z.L., P.C. and T.L.; writing—review and editing, Y.Z. and R.L.; visualization, Z.L.; supervision, T.L.; project administration, P.C.; funding acquisition, Y.Z., L.H. and R.L. All authors have read and agreed to the published version of the manuscript.

Funding: This work was funded by the National Natural Science Foundation of China (grant no. 52371032), a research project funded by the Education Department of Hunan Province (grant no. 23B0499), the Project of the State Key Laboratory of Precision Manufacturing for Extreme Service Performance, Central South University (grant no. ZZYJKT2021-01), and a Hengyang City research project of the Science and Technology Bureau (grant no. 202150063472).

Institutional Review Board Statement: Not applicable.

Informed Consent Statement: Not applicable.

Data Availability Statement: Data are contained within the article.

Conflicts of Interest: Author Tijun Li was employed by the State-Owned Sida Machinery Manufacturing Company. The remaining authors declare that the research was conducted in the absence of any commercial or financial relationships that could be construed as a potential conflict of interest.

References

1. Wu, Z.; Kou, H.; Chen, N.; Xi, Z.; Fan, J.; Tang, B.; Li, J. Recent developments in cold dwell fatigue of titanium alloys for aero-engine applications: A review. *J. Mater. Res. Technol.* **2022**, *20*, 469–484. [CrossRef]
2. Alipour, S.; Moridi, A.; Liou, F.; Emdadi, A. The Trajectory of Additively Manufactured Titanium Alloys with Superior Mechanical Properties and Engineered Microstructures. *Addit. Manuf.* **2022**, *60*, 103245. [CrossRef]
3. Zhao, Q.; Sun, Q.; Xin, S.; Chen, Y.; Wu, C.; Wang, H.; Xu, J.; Wan, M.; Zeng, W.; Zhao, Y. High-strength titanium alloys for aerospace engineering applications: A review on melting-forging process. *Mater. Sci. Eng. A* **2022**, *845*, 143260. [CrossRef]
4. Tshephe, T.S.; Akinwamide, S.O.; Olevsky, E.; Olubambi, P.A. Additive manufacturing of titanium-based alloys- A review of methods, properties, challenges, and prospects. *Heliyon* **2022**, *8*, e09041. [CrossRef] [PubMed]
5. Yang, C.; Cui, S.; Wu, Z.; Zhu, J.; Huang, J.; Ma, Z.; Fu, R.K.Y.; Tian, X.; Chu, P.K.; Wu, Z. High efficient co-doping in plasma electrolytic oxidation to obtain long-term self-lubrication on Ti6Al4V. *Tribol. Int.* **2021**, *160*, 107018. [CrossRef]
6. Shi, Y.; Gong, S.; Xu, H.; Wang, Z.; Yang, G.; Qi, B. Alloying strategies for additive manufacturing of Ti6Al4V based alloys, composites and functionally graded materials: Microstructure and phase evolution of intra and inter-layer. *J. Mater. Res. Technol.* **2023**, *27*, 6225–6263. [CrossRef]
7. Murmu, A.M.; Parida, S.K.; Das, A.K.; Kumar, S. Evaluation of laser cladding of Ti_6Al_4V-ZrO_2-CeO_2 composite coating on Ti6Al4V alloy substrate. *Surf. Coat. Technol.* **2023**, *473*, 129988. [CrossRef]
8. Suo, H.; Wei, Z.; Luo, B.; Wang, L.; Zhang, K.; Liang, B.; Deng, K.; Cheng, H. Interfacial wear damage mechanism between Ti-alloy and Al-alloy in interference-fit joint and influence of surface coatings: Experimental and numerical study. *Eng. Fail. Anal.* **2023**, *143*, 106931. [CrossRef]
9. Asl, H.G.; Sert, Y.; Küçükömeroğlu, T.; Bayrak, Ö. The comparison of wear performances of CP-Ti, Ti6Al4V, Ti45Nb alloys oxidized by anodic oxidation under ambient air and vacuum conditions. *Mater. Today Commun.* **2023**, *34*, 105466. [CrossRef]
10. Suo, H.; Wei, Z.; Zhang, K.; Deng, K.; Cheng, H.; Luo, B.; Li, H.; Wang, L.; Liang, B. Interfacial wear damage of CFRP/Ti-alloy single-lap bolted joint after long-term seawater aging. *Eng. Fail. Anal.* **2022**, *139*, 106464. [CrossRef]
11. Wu, F.; Zhang, N.; Sun, Y.; Li, X.; Liu, Z.; Yang, Y. Effect of applied load on tribological behaviour of Ti–48Al–2Cr–2Nb alloy under oil-lubricated condition. *Wear* **2024**, *538–539*, 205210. [CrossRef]
12. Chen, P.; Li, B.; Liu, Z.; Zhou, Y.; Li, R.; Zhang, Y. High-temperature oxidation behaviors and mechanical properties of TiAlCrMn HEAs during heat treatment. *Trans. Nonferrous Met. Soc. China* **2024**, *34*, 237–252.
13. Wei, Q.; Zhang, A.; Han, J.; Xin, B.; Su, B.; Wang, X.; Ma, Q.; Meng, J. Development of a $Ti_{30}Hf_{20}Nb_{20}Ta_{10}V_{10}Mo_7W_3$ refractory high entropy alloy with excellent mechanical properties and wear resistance. *J. Alloys Compd.* **2023**, *966*, 171571. [CrossRef]
14. Lu, X.; Zhang, D.; Xu, W.; Yu, A.; Zhang, J.; Tamaddon, M.; Zhang, J.; Qu, X.; Liu, C.; Su, B. The effect of Cu content on corrosion, wear and tribocorrosion resistance of Ti-Mo-Cu alloy for load-bearing bone implants. *Corros. Sci.* **2020**, *177*, 109007. [CrossRef]
15. Xiang, K.; Chai, L.; Zhang, C.; Guan, H.; Wang, Y.; Ma, Y.; Sun, Q.; Li, Y. Investigation of microstructure and wear resistance of laser-clad CoCrNiTi and CrFeNiTi medium-entropy alloy coatings on Ti sheet. *Opt. Laser Technol.* **2022**, *145*, 107518. [CrossRef]
16. Waghmare, D.T.; Kumar Padhee, C.; Prasad, R.; Masanta, M. NiTi coating on Ti-6Al-4V alloy by TIG cladding process for improvement of wear resistance: Microstructure evolution and mechanical performances. *J. Mater. Process. Technol.* **2018**, *262*, 551–561. [CrossRef]
17. Wu, Y.; Wang, A.H.; Zhang, Z.; Xia, H.B.; Wang, Y.N. Microstructure, wear resistance and cell proliferation ability of in situ synthesized Ti–B coating produced by laser alloying. *Opt. Laser Technol.* **2015**, *67*, 176–182. [CrossRef]

18. Wang, X.-Q.; Zhang, Y.-S.; Han, W.-Z. Design of high strength and wear-resistance β-Ti alloy via oxygen-charging. *Acta Mater.* **2022**, *227*, 117686. [CrossRef]
19. Yin, M.-g.; Cai, Z.-b.; Li, Z.-y.; Zhou, Z.-r.; Wang, W.-j.; He, W.-f. Improving impact wear resistance of Ti-6Al-4V alloy treated by laser shock peening. *Trans. Nonferrous Met. Soc. China* **2019**, *29*, 1439–1448. [CrossRef]
20. Revankar, G.D.; Shetty, R.; Rao, S.S.; Gaitonde, V.N. Wear resistance enhancement of titanium alloy (Ti–6Al–4V) by ball burnishing process. *J. Mater. Res. Technol.* **2017**, *6*, 13–32. [CrossRef]
21. Liu, L.; Shen, H.H.; Liu, X.Z.; Guo, Q.; Meng, T.X.; Wang, Z.X.; Yang, H.J.; Liu, X.P. Wear resistance of TiN(Ti2N)/Ti composite layer formed on C17200 alloy by plasma surface Ti-alloying and nitriding. *Appl. Surf. Sci.* **2016**, *388*, 103–108. [CrossRef]
22. Rossi, M.C.; Bazaglia Kuroda, P.A.; Solano de Almeida, L.; Rossino, L.S.; Moreira Afonso, C.R. A detailed analysis of the structural, morphological characteristics and micro-abrasive wear behavior of nitrided layer produced in α (CP–Ti), α+β (Ti–6Al–4V), and β (TNZ33) type Ti alloys. *J. Mater. Res. Technol.* **2023**, *27*, 2399–2412. [CrossRef]
23. Li, Z.-y.; Cai, Z.-b.; Wu, Y.-p.; Zhu, M.-h. Effect of nitrogen ion implantation dose on torsional fretting wear behavior of titanium and its alloy. *Trans. Nonferrous Met. Soc. China* **2017**, *27*, 324–335. [CrossRef]
24. Wu, H.; Xi, K.; Xiao, S.; Qasim, A.M.; Fu, R.K.Y.; Shi, K.; Ding, K.; Chen, G.; Wu, G.; Chu, P.K. Formation of self-layered hydrothermal coating on magnesium aided by titanium ion implantation: Synergistic control of corrosion resistance and cytocompatibility. *Surf. Coat. Technol.* **2020**, *401*, 126251. [CrossRef]
25. Naeem, M.; Awan, S.; Shafiq, M.; Raza, H.A.; Iqbal, J.; Díaz-Guillén, J.C.; Sousa, R.R.M.; Jelani, M.; Abrar, M. Wear and corrosion studies of duplex surface-treated AISI-304 steel by a combination of cathodic cage plasma nitriding and PVD-TiN coating. *Ceram. Int.* **2022**, *48*, 21473–21482. [CrossRef]
26. Guo, J.; Shi, Y.; Li, C.; Zhang, G. Investigation of nitrogen ionization state and its effect on the nitride layer during fiber laser gas nitriding of Ti-6Al-4V alloy. *Surf. Coat. Technol.* **2021**, *418*, 127254. [CrossRef]
27. Chen, P.; Wu, W.; Liu, H.; Li, H.; Qiu, C. Metastable FeCrMnCo HEAs with the reinforcement of tungsten carbide fabricated by laser melting: Microstructure, mechanical properties and tribological behaviors. *Mater. Charact.* **2023**, *206*, 113397. [CrossRef]
28. Chen, P.-h.; Zhang, Y.; Li, R.-q.; Liu, Y.-x.; Zeng, S.-s. Influence of carbon-partitioning treatment on the microstructure, mechanical properties and wear resistance of in situ VCp-reinforced Fe-matrix composite. *Int. J. Miner. Metall. Mater.* **2020**, *27*, 100–111. [CrossRef]
29. Chen, P.; Liu, Z.; Li, R.; Li, X. The effect of manganese additions on the high temperature oxidation behaviour of the high-vanadium cast iron. *J. Alloys Compd.* **2018**, *767*, 181–187. [CrossRef]
30. Pede, D.; Li, M.; Virovac, L.; Poleske, T.; Balle, F.; Müller, C.; Mozaffari-Jovein, H. Microstructure and corrosion resistance of novel β-type titanium alloys manufactured by selective laser melting. *J. Mater. Res. Technol.* **2022**, *19*, 4598–4612. [CrossRef]
31. Patel, P.; Zala, A.; Parekh, T.; Kahar, S.D.; Jamnapara, N.I. High temperature oxidation behavior of thermal and plasma processed aluminide coated Ti6Al4V alloys. *Surf. Coat. Technol.* **2022**, *447*, 128839. [CrossRef]
32. Sun, F.; Liu, X.-L.; Luo, S.-Q.; Xiang, D.-D.; Ba, D.-C.; Lin, Z.; Song, G.-Q. Duplex treatment of arc plasma nitriding and PVD TiN coating applied to dental implant screws. *Surf. Coat. Technol.* **2022**, *439*, 128449. [CrossRef]